PERGAMON

International Journal of Multiphase Flow 26 (2000) 763–781

International Journal of Multiphase Flow

www.elsevier.com/locate/ijmulflow

Solid fraction fluctuations in solid–liquid flows

Roberto Zenit*, Melany L. Hunt

Mechanical Engineering Department, California Institute of Technology, Pasadena, CA 91125, USA

Received 24 February 1998; received in revised form 1 June 1999

Abstract

The fluctuating component of the solid fraction is studied for liquid–solid mixtures using an impedance volume-fraction meter (IVFM). The experiments involve a vertical gravity driven flow using glass particles in water, and a liquid fluidized bed with either glass, steel or nylon particles. The signals of the IVFMs for different flow conditions are analyzed in time and frequency domains. Results show that the magnitude of the root-mean-square (RMS) solid fraction fluctuation increases from low concentrations ($<10\%$ solid fraction), reaches a local maximum at approximately 30% solid fraction, decreases again and reaches a maximum at concentrations around 45%. For higher concentrations, the RMS fluctuations decreases until the packed state. For the same solid fraction the magnitude of the fluctuation increases for larger diameter particles. Two main types of fluctuations were identified: large-amplitude low-frequency fluctuations and small-amplitude high-frequency fluctuations. The low-frequency fluctuations were dominant at high concentrations ($>30\%$), while the high-frequency fluctuations became more prominent for concentrations below 30%. When the low frequency fluctuations were filtered out and the RMS fluctuation was re-calculated the scaling appear to change: the filtered RMS fluctuations were larger for experiments with higher particle inertia. A comparison between the filtered RMS solid fluctuations and an exiting model showed limited agreement.

Keywords: Solid–liquid flows; Solid fraction fluctuation; Particle collisions

* Corresponding author. Tel.: +1-607-255-5882; fax: +1-607-255-9166.
E-mail address: zenit@cheme.cornell.edu (R. Zenit).

0301-9322/00/$ - see front matter
PII: S0301-9322(99)00066-X

1. Introduction

Dispersed solid–liquid mixtures are inherently unsteady. Experimental and industrial applications provide evidence to show that the velocities of both the fluid and solid phases and their respective volume fractions experience important fluctuations around their mean values. Because of this agitation, the effective coefficients of heat and mass transfer have extremely high values; hence, these systems are of interest for many engineering applications. Multiple factors determine the nature of these fluctuations, such as the upstream and downstream conditions, the density ratio of the phases and the mean slip velocity. The interaction between the phases is complex, and significant momentum is transferred between the phases and with the boundaries.

The steady behavior of liquid fluidized systems has received a considerable amount of attention (Di Felice, 1995). The unsteady behavior can be characterized according to the nature of the solid fraction fluctuations. In general, solid fraction fluctuations can be divided in two categories based on their amplitude and frequency (Couderc, 1985). Most of studies dealing with the unsteady behavior of solid–liquid systems deal with the formation of large global fluctuations, which include those disturbances related to 'bubbles' in fluidized beds. These large-amplitude (low-frequency) disturbances, or waves, have been studied intensively from the stability point of view (Jin, 1996; Ham et al., 1990; Batchelor, 1988) and are strongly dependent on external conditions, such as the geometry of container or characteristics of the fluid distribution system, etc. Less attention has been focused on the study of the small-scale fluctuations. Small scale fluctuations (high-frequency) are induced by inter-phase interactions, local hydrodynamics, and presumably particle collisions (Buyevich and Kapbasov, 1994). Although some early theoretical studies suggest that particles immersed in a liquid would not undergo direct collisions, in real flows, particles do collide and rebound even when the characteristic particle Stokes number is as low as of order one (Zenit and Hunt, 1999). Particle collisions have also been identified to generate stresses in flowing solid–liquid mixtures (Zenit et al., 1997).

Didwania and Homsy (1981) performed a detailed analysis of the flow regimes and transitions in liquid fluidized beds. Using an optical technique, they characterized four distinct regimes, in terms of the time and length scales of the particle motion. The regimes include (in the order of decreasing solid fraction), wavy flow, wavy flow with transverse structure, fine scale turbulent flow and bubbling states.

By measuring the instantaneous cross-section averaged impedance of the solid–liquid mixture, a measure of the solid fraction is obtained. This non-intrusive technique provides information of the time-dependent structure of the fluidized media. The mean and root mean squared components of the solid fraction are analyzed in both time and frequency domains. Experiments were performed in a liquid fluidized bed and in a vertical gravity-driven liquid–solid flow. The variance of the measured time-signal was obtained for different particle sizes and densities, and for two different test section diameters. The presented experimental results corroborate the behavior previously reported by Didwania and Homsy (1981) and expands on this work by considering particles of different diameters and densities, and by identifying and measuring the high frequency solid fraction fluctuations. By means of a digital filtering technique, the high frequency solid fraction fluctuations were isolated from those resulting

from the bulk bed behavior. Their magnitude is compared with the theoretical predictions of an exiting model, and clearly show an increase with increasing Stokes number.

2. Experiments

Experiments were performed in the facility shown in Fig. 1. The working section was fabricated out of transparent lucite to facilitate the visual observation of the flowing mixtures. Prior to an experiment the particles were stored in a bin on top of the working section. By setting the aperture of the solids feeder and the downstream water valves, cocurrent and counter-current flows could be generated for a wide range of solid fractions. Also, by installing a screen and a flow straightener at the bottom of the working section, the system could be operated as a fluidized bed. Details of the experimental apparatus can be found in Zenit (1998). The particles employed were nearly mono-disperse spherical particles. Properties of the particles are listed in Table 1, including the density ratio of the solid to fluid phases, ρ_s/ρ_f, the particle terminal velocity, u_t, the terminal Reynolds number. $Re_t = \rho_f u_t d/\mu_f$ and terminal Stokes number, $St_t = (\rho_s/\rho_f)Re_t/9$. The fluid used for all of the experimental measurements was tap water.

An Impedance Volume Fraction Meter (IVFM) developed by Kytömaa and Brennen (1986) and Bernier (1982) is used to measure the instantaneous volume fraction. This non-intrusive instrument is based on the measurement of the high-frequency electric impedance of the mixture and consists of two shielded stainless steel electrodes laid flush with the

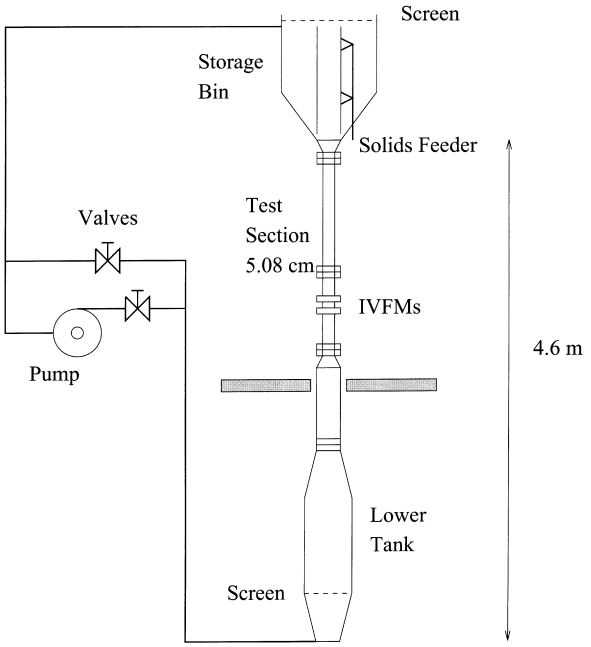

Fig. 1. Experimental setup.

Table 1
Properties of particles used in experiments

Material	d (mm)	ρ_s/ρ_f	u_t (cm/s)	Re_t	St_t
Glass (×)	3.00	2.54	31.8	954	269
Glass (○)	6.00	2.54	47.4	2583	726
Steel (◇)	4.50	7.78	89.6	3665	2303
Nylon (△)	6.35	1.14	13.6	78.5	99
PVC (+)	3.41[a]	1.43	16.0	440	69

[a] Equivalent diameter. Cylindrical shape.

interior surface of the tube. The meter provides a cross-sectional average measurement of the impedance in the test section. To provide a high-frequency response, the measuring electronics use a 50 kHz excitation and a double bridge signal processor. Due to the shielded configuration of the electrodes, the spatial resolution is a few centimeters. Details on the electronics and the implementation of this measuring system can be found in the references. Sets of electrodes were used in both a 5.08 cm and a 10.16 cm diameter test sections.

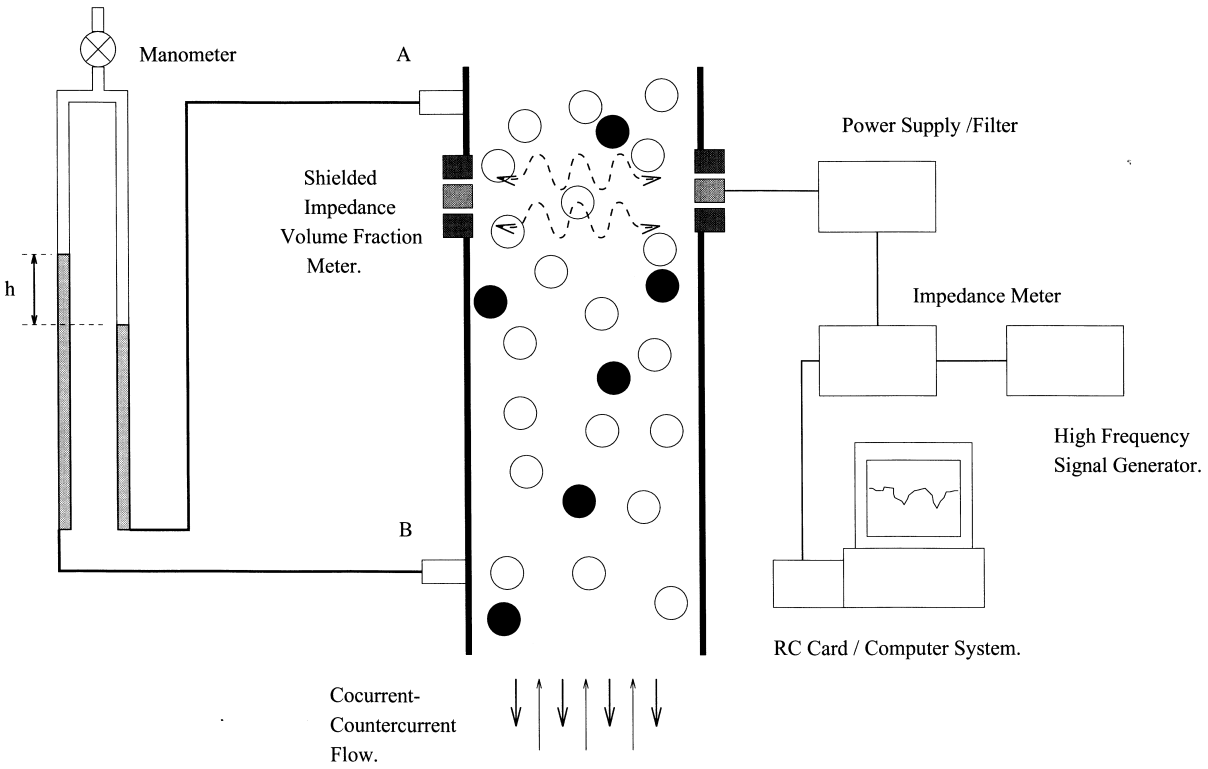

Fig. 2. Experimental setup to measure the fluctuations of the solid fraction signal in a liquid–solid flow.

To calibrate the IVFM, a manometer was connected to the test section as shown in Fig. 2. The solid fraction, ν, was determined from the hydrostatic pressure gradient in the two-component medium obtained from the manometer reading. If h' is the distance between points A and B and h is the difference in the manometer levels, then in the absence of frictional effects, the solid fraction is given by

$$\nu = \frac{h}{h'(\rho_s/\rho_f - 1)} \tag{1}$$

where ρ_s is the density of the particles and ρ_f is the density of the fluid. Fig. 3 shows a typical calibration for 3 mm glass spheres in a 10.16 cm test section. The response of the meters is linear for the entire range of concentrations. The same linear response was obtained for all the particles tested. The dynamic response of the meter can be quantified by obtaining the decay time of the autocorrelation function of the impedance-time signal of the flowing mixtures and is discussed in detail by Kytömaa (1987).

The root-mean-square (RMS) fluctuation of the solid fraction, $\overline{\nu'}$, is calculated as

$$\overline{\nu'} = \sqrt{\frac{1}{N}\sum_{i=1}^{N}(\bar{\nu} - \nu_i)^2} \tag{2}$$

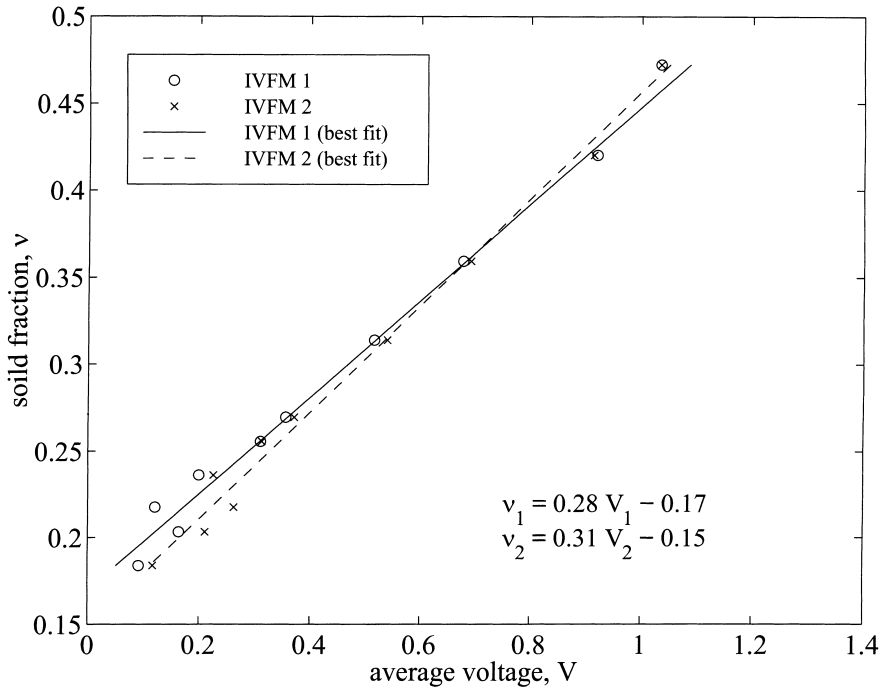

Fig. 3. Typical calibration of the impedance volume fraction meters. 3 mm glass particles in a 10.18 cm test section liquid fluidized bed.

where $\bar{\nu}$ is the average solid fraction and N is the number of samples of the instantaneous solid fraction. The measurements were obtained by setting a certain sampling rate and length of sample in the data acquisition system. The sampling rate for all the results presented was chosen to be 1 kHz. Samples of at least 8000 data points (8 s at 1 kHz) were used for the calculations. Longer recording times would be more appropriate to capture the behavior of the low frequency solid fraction fluctuations: however, since here the emphasis is on the high-frequency component of the fluctuations, short recording times at high sampling rates suffice to obtain the desired information.

The measurement of the unsteady component of the volume fraction was first proposed and used by Kytömaa (1987). In that investigation, the solid fraction fluctuations were used to measure small-amplitude wave propagation velocities in two and three components flows. In this paper, the emphasis is not on wave propagation or stability. The technique is used to measure the amount of agitation in solid–liquid flows to investigate the flow regime transitions. The information is also pertinent in identifying the generating mechanisms of the particle pressure (Zenit et al., 1997).

3. Results

3.1. Liquid fluidized beds

For the first part of this study the experiment was operated as a liquid fluidized bed. The particles were placed in the test section and by controlling the liquid flow rate, different steady state mixtures could be achieved. In most cases the measurement was taken a number of times to ensure repeatability.

Figs. 4–7 show typical cases of the fluctuating volume fraction signals for a fluidized bed over a range of particle densities and diameters. The figures show, on the left column, the solid fraction fluctuation, $\nu - \bar{\nu}$, measured as a function of time for different mean solid fractions. On the right frequency transformed signals are shown from a fast Fourier transform routine. The vertical axis of the frequency domain plots can be interpreted as the energy of the fluctuations.

Fig. 4 shows the results obtained for 3 mm glass particles in a 5.08 cm diameter test section. The presence of large-scale fluctuations can be readily observed at high concentrations. These low frequency waves can be observed in the experiment as upwards moving regions of lower concentration. As the solid fraction decreases, these waves become more irregular as higher frequency fluctuations begin to appear. For most concentrations the low frequency fluctuations contain the most energy. As the concentration decreases, the fluctuation energy is distributed into a wider range of frequencies. The sharp spike at 60 Hz is most likely the result of electronic noise.

Fig. 5 shows the results for 6 mm glass spheres fluidized in a 5.08 cm test section. For the case of the highest concentration, the large scale disturbances begin to appear. This concentration (51%) is just beyond that of the incipient fluidization for this flow. The large-scale fluctuations seem to be of larger magnitudes than those of the 3 mm glass case. As in the previous case, a decrease in the mean solid fraction results in higher frequency.

The results obtained for fluidized 6.35 mm nylon spheres are shown in Fig. 6. Large scale fluctuations are observed for most concentrations, and high frequency fluctuations appear to be less evident than in the two previous cases.

Fig. 7 presents the measurements for the 4.5 mm steel particles. Similar to the previous

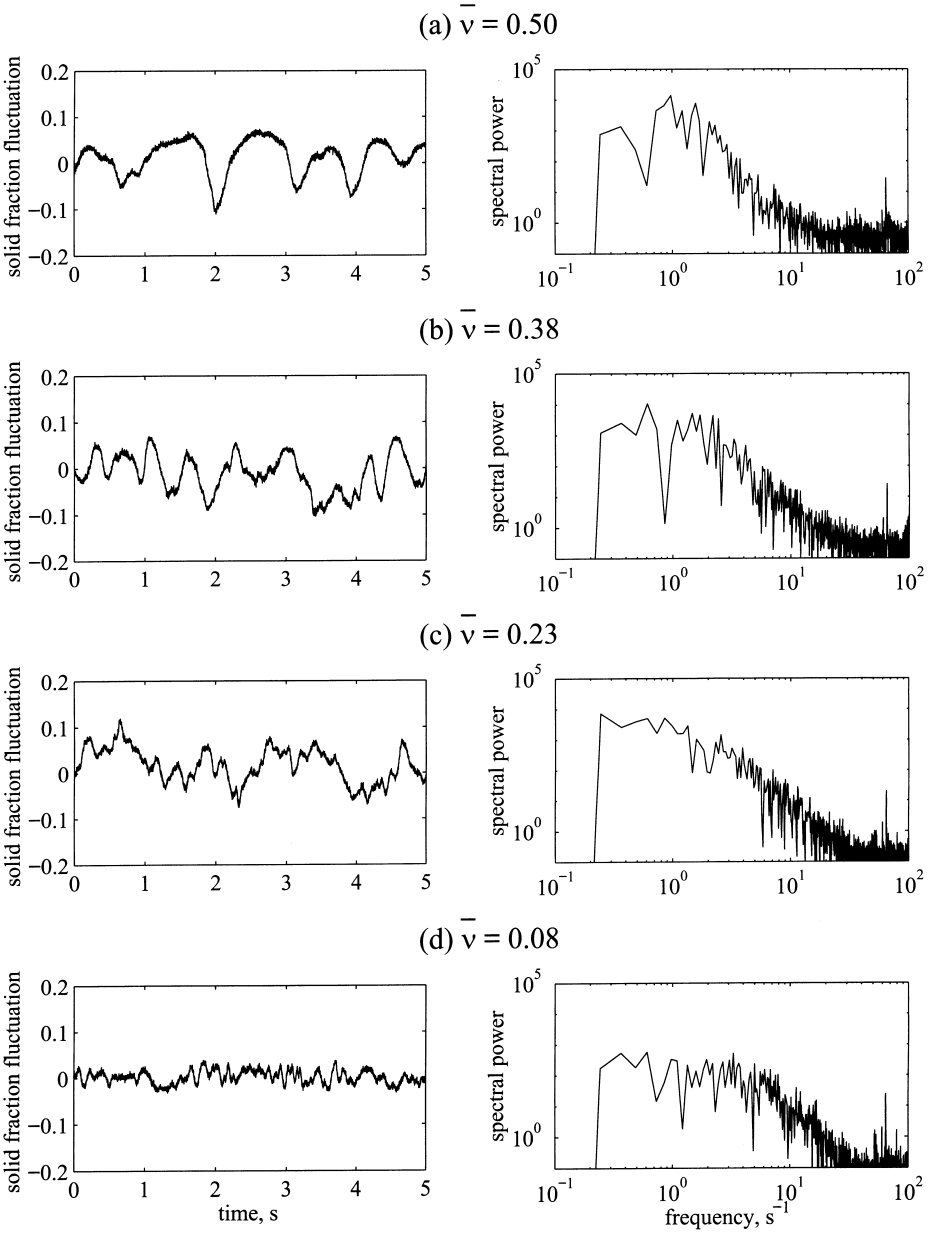

Fig. 4. Time and frequency domain volume fraction fluctuation, $\nu - \bar{\nu}$, traces for a liquid fluidized 3 mm glass particles in a 5.08 cm diameter test section.

cases, large-scale fluctuations are observed in concentrated beds. The upward-traveling regions of low concentrations were observed for overall concentrations higher than 30%. The RMS fluctuation values measured for this case were the largest of all the cases tested.

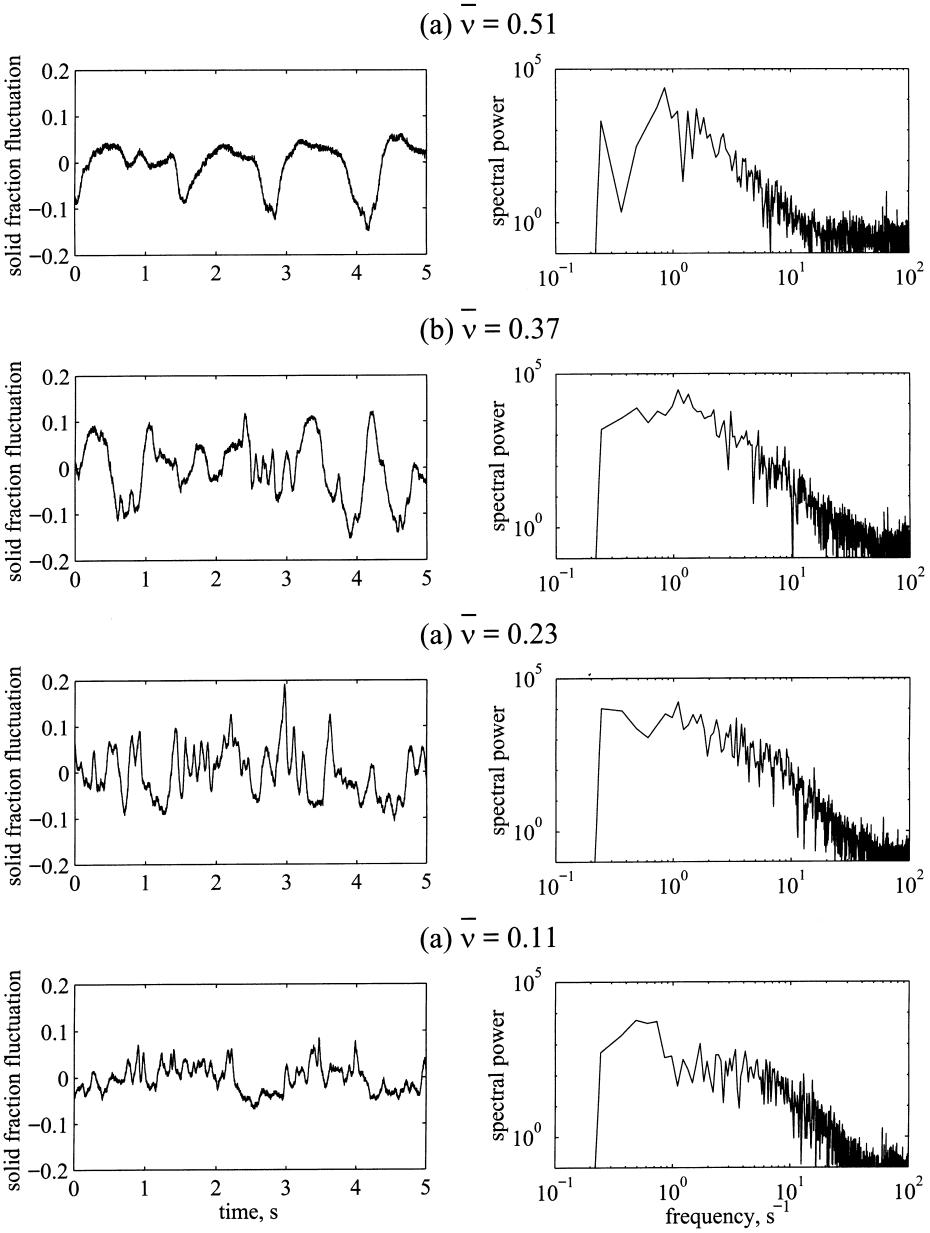

Fig. 5. Time and frequency domain volume fraction fluctuation, $\nu - \bar{\nu}$, traces for liquid fluidized 6 mm glass particles in a 5.08 cm diameter test section.

For all the particles tested in the 5.08 cm test section, the RMS solid fraction fluctuations, as calculated from Eq. (2), and are presented in Fig. 8 as a function of the mean solid fraction. In a packed state, when the fluid velocity has just reached the minimum fluidization velocity, the amount of fluctuation is small. As the solid fraction decreases, the RMS fluctuation increases

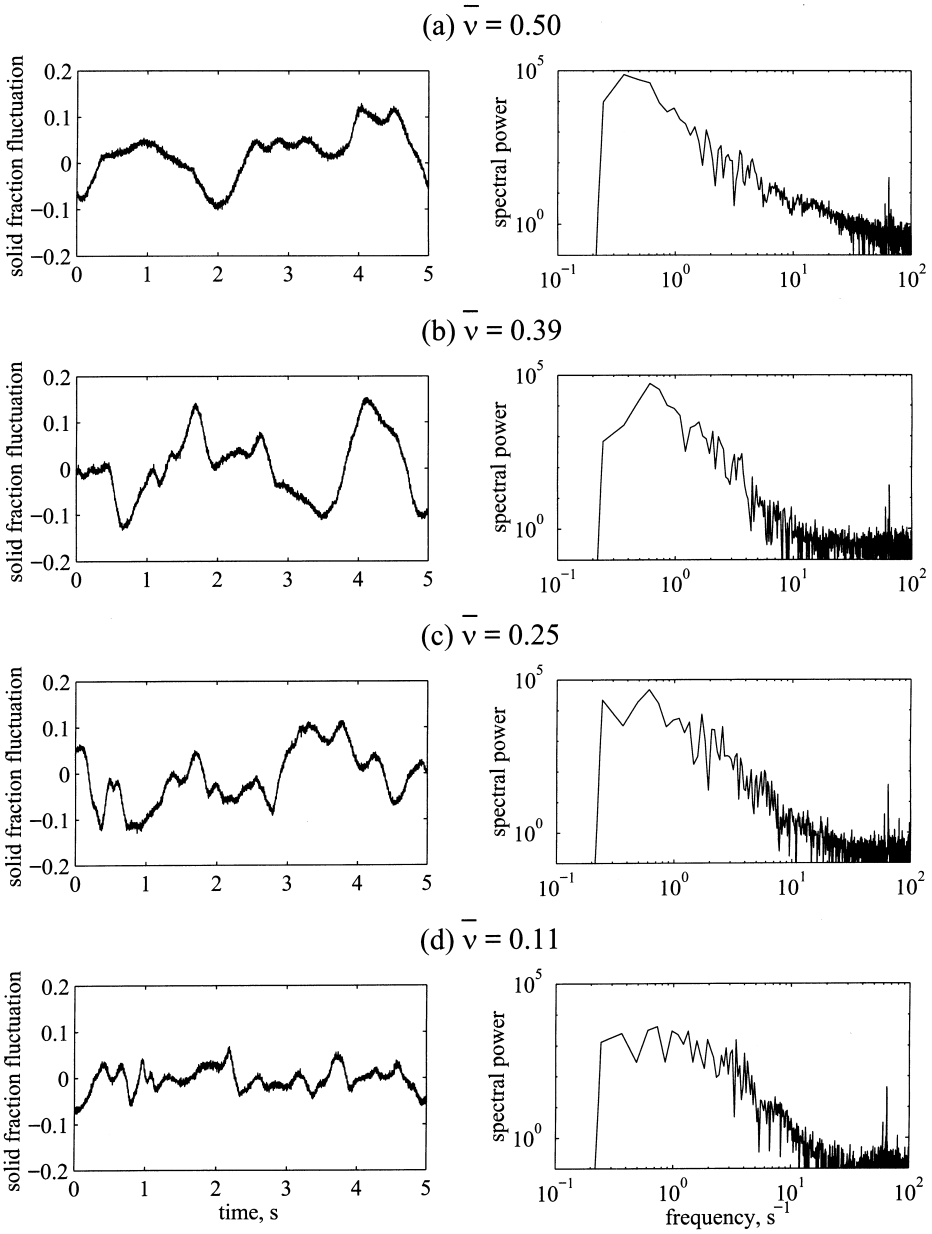

Fig. 6. Time and frequency domain volume fraction fluctuation, $\nu - \bar{\nu}$ traces for liquid fluidized 6.35 mm nylon particles in a 5.08 cm diameter test section.

rapidly and reaches a local maximum at concentrations of approximately 45%. The aforementioned large-scale fluctuations, or concentration waves, are the main cause of this rapid increase in the RMS fluctuation. The magnitude of the concentration waves decreases as the solid fraction is further reduced, and the small-scale fluctuations begin to appear. Around a

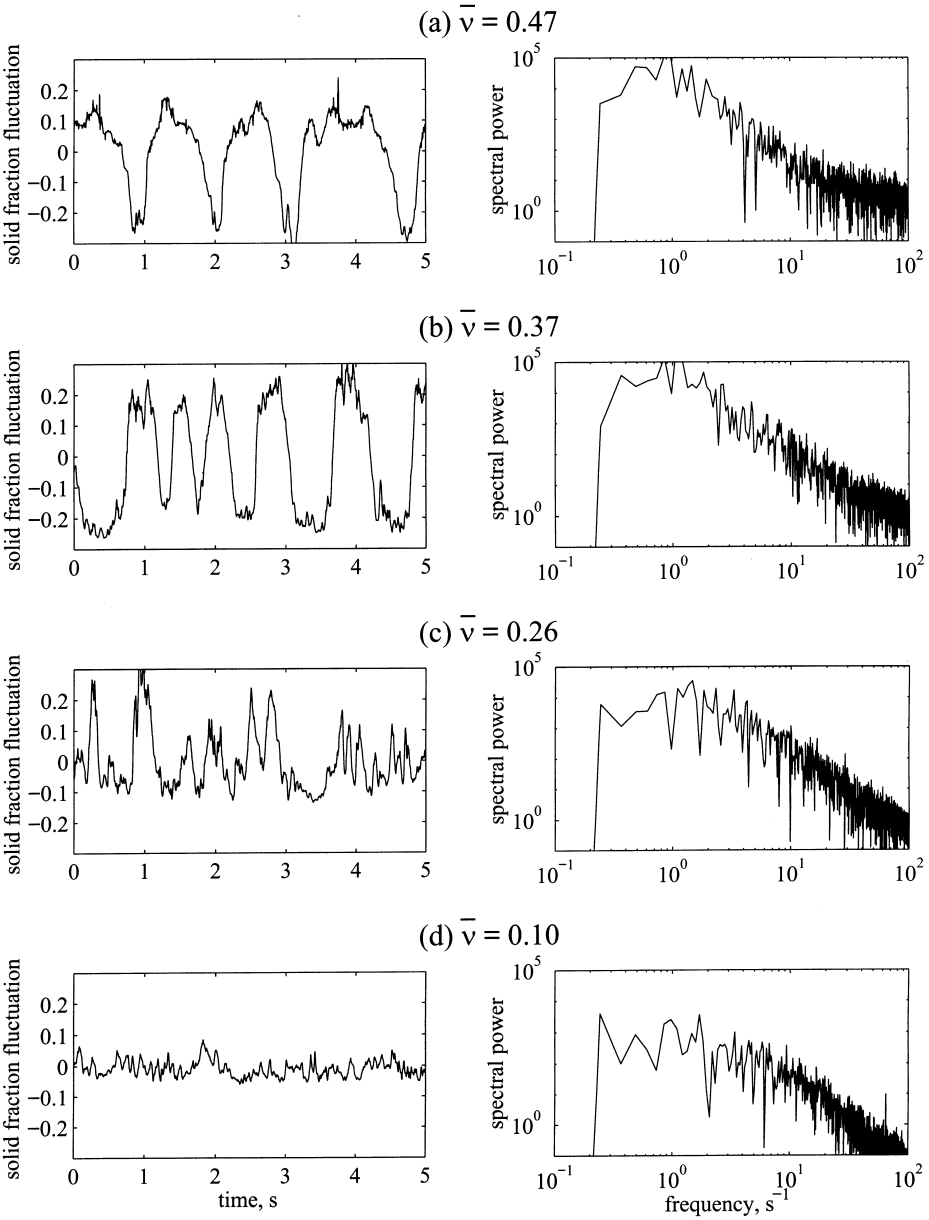

Fig. 7. Time and frequency domain volume fraction fluctuation, $\nu - \bar{\nu}$, traces for liquid fluidized 4.5 mm steel particles in a 5.08 cm diameter test section.

solid fraction of 30%, another local maximum in the RMS fluctuation appears. In this range of concentrations, the small-scale fluctuations appear to be dominant. For concentrations lower than 30%, the RMS fluctuation decreases again. For dilute mixtures the agitation and the collision frequency decreases due to the small number of particles. The same behavior was found for all of the particles tested. The magnitude of the RMS fluctuation appears to be larger for particles of larger diameter, with the exception of the 4.5 mm steel particles, which are the densest of all the particles tested. For comparison, the experimental measurements of the RMS solid fraction fluctuation by Didwania and Homsy (1981) are also shown (filled symbols). Only their results for the case 1.1 mm ballotine spheres were found to have a terminal Stokes number in the same range as in the experiments presented here. For that case, the comparison shows good agreement; however, Didwania and Homsy reported results only for a narrow range of solid fractions.

Tests were performed in two distinct test sections for the same particles. Fig. 9 shows comparisons of the measurements for 3 mm glass particles in a 5.08 cm and a 10.16 cm diameter test sections. Clearly, the results show that the larger test section has no significant effect on the magnitude of the RMS solid fraction fluctuations, at least for this particular case.

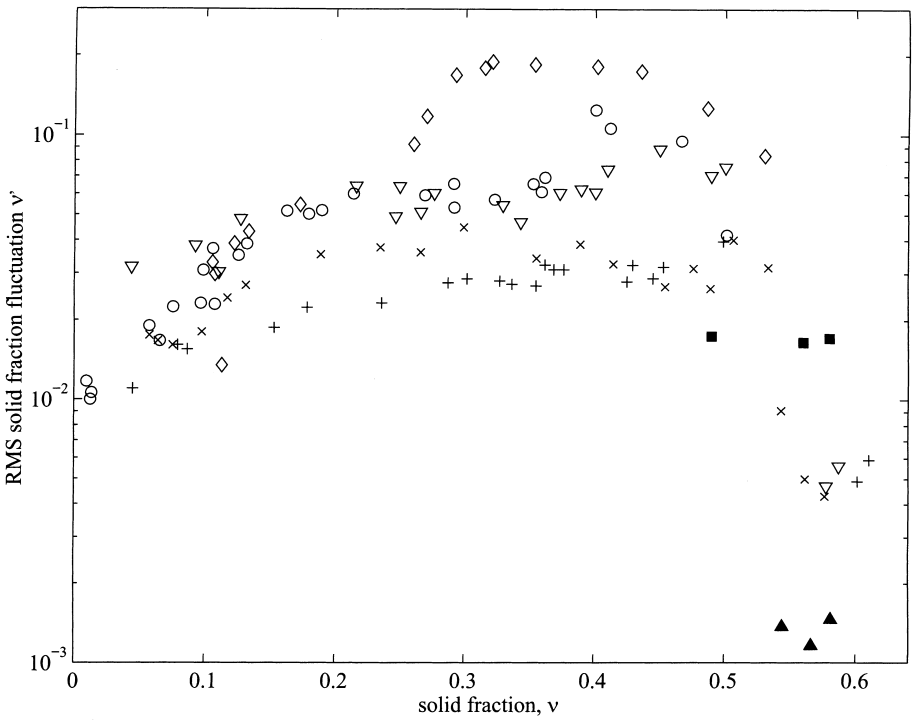

Fig. 8. RMS solid fraction fluctuation as a function of the solid fraction. Liquid fluidized particles in a 5.08 cm test section: 3 mm glass particles (×), 6 mm glass particles (○), 4.5 mm steel particles (◇), 6.35 mm nylon particles (▽), and 3.41 mm PVC cylinders (+). The filled symbols show the experimental results of Didwania and Homsy (1981): 1.1 mm ballotine particles (■, $St_t \approx 105$), 0.59 mm ballotine particles (▲,$St_t \approx 32$).

3.2. Vertical gravity driven flow

This section examines the influence of the flow direction on the magnitude of the solid fraction fluctuations. In contrast with the fluidized bed setup, the net velocity of the solid phase for this set of results is not zero. Since the experiment is gravity driven, the net velocity of the particles is always negative (negative is in the downwards direction). Depending on the valve arrangement in the experiment, the liquid could be allowed to flow in the direction of the particles (cocurrent flow) or in the opposite direction (countercurrent flow). For the gravitational flows only 3 mm glass spheres were tested.

Fig. 10 shows the measured fluctuations as a function of the solid fraction for the two test sections and for both cocurrent and countercurrent flow. The data for all the experimental sets appears to have a maximum at a solid fraction of approximately 25%. For most concentrations the RMS fluctuation is larger for countercurrent flows. The measurements of the cocurrent flow in the 5.08 cm test section appear to have the smallest value of RMS fluctuation.

4. Low and high frequency fluctuations

Figs. 4–7 clearly show the two types of fluctuations. Low frequency waves can be considered a global phenomena of the particle ensemble, while high frequency fluctuations can be related to local variations of the particle-scale hydrodynamics. To study each of these contributions to the total RMS solid fraction fluctuation, a digital filtering analysis is performed.

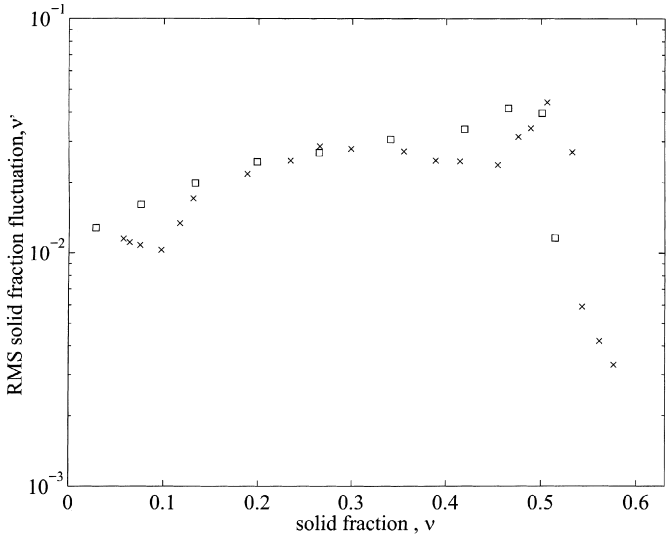

Fig. 9. RMS solid fraction fluctuation as a function of the solid fraction. Liquid fluidized 3 mm glass particles in the 5.08 cm (×) and the 10.16 cm (□) test sections.

To eliminate the low frequency component from the solid fraction signals, a high-pass filtering algorithm is applied to the time-dependent traces. The digital filter models a high pass fourth order Butterworth filter. A cut-off frequency of 3 Hz was chosen by examining the frequency-transformed signals. Fig. 11 shows the effect of the filter on the volume fraction fluctuation signals obtained for the 3 mm glass particles in a fluidized bed. On the left the original time signal is shown, and on the right the signal after the filtering. The low-frequency events appear to be completely eliminated. The lowest concentration case is not affected significantly by the filtering algorithm.

Fig. 12 shows the effect of the filter on the magnitude of the calculated RMS solid fraction fluctuation, for the case of 3 mm glass fluidized particles. The magnitude of the RMS solid fraction fluctuation decreases as a result of the filtering. The local maximum that was observed at high concentrations disappears after the filtering. The measurements preserve the presence of a maximum at a concentration of approximately 30%.

The filtering algorithm was applied to the solid fraction traces of all the other particles tested. The results of the RMS solid fraction fluctuation as a function of solids concentrations are shown in Fig. 13. Clearly, the overall magnitude of the RMS solid fraction fluctuation for all the cases is reduced by almost an order of magnitude, with the exception of the steel particles; however, the appearance of a maximum at approximately 30% of concentration is preserved. The dependence of the RMS fluctuation on the particle size observed from the unfiltered data changes. Before filtering, the data for the particles of larger diameter appear to have larger fluctuations. After filtering, for a given concentration, the RMS fluctuation clearly increases with the Stokes number. The only exception to this trend was observed in the 3.41

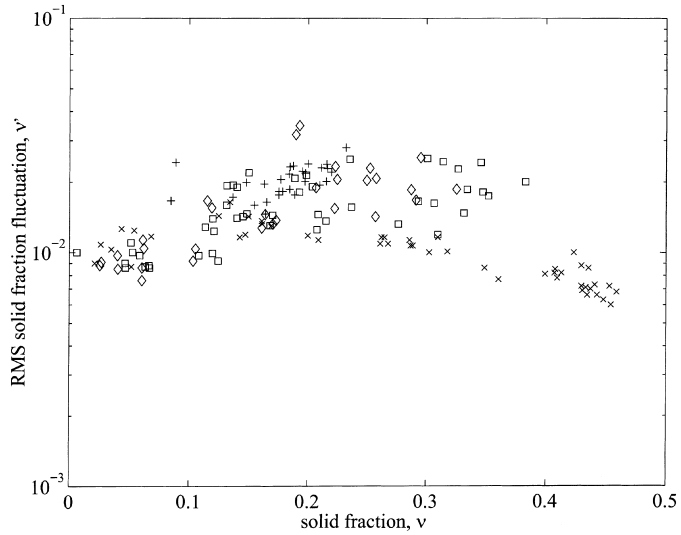

Fig. 10. RMS solid fraction fluctuation as a function of the solid fraction. Vertical flow of 3 mm glass particles in both test sections (TS). (×) cocurrent flow in 5.08 cm TS, (+) countercurrent flow in 5.08 cm TS. (□) cocurrent flow in 10.2 cm TS. (◇) countercurrent flow in 10.2 cm TS.

mm PVC cylindrical particles. Although these particles have the smallest Stokes number of all particles tested, the filter RMS fluctuation was found to be higher that of the 6.35 mm Nylon particles for all concentrations. This disagreement can be an indication of the influence of the shape of the particles in the measurements.

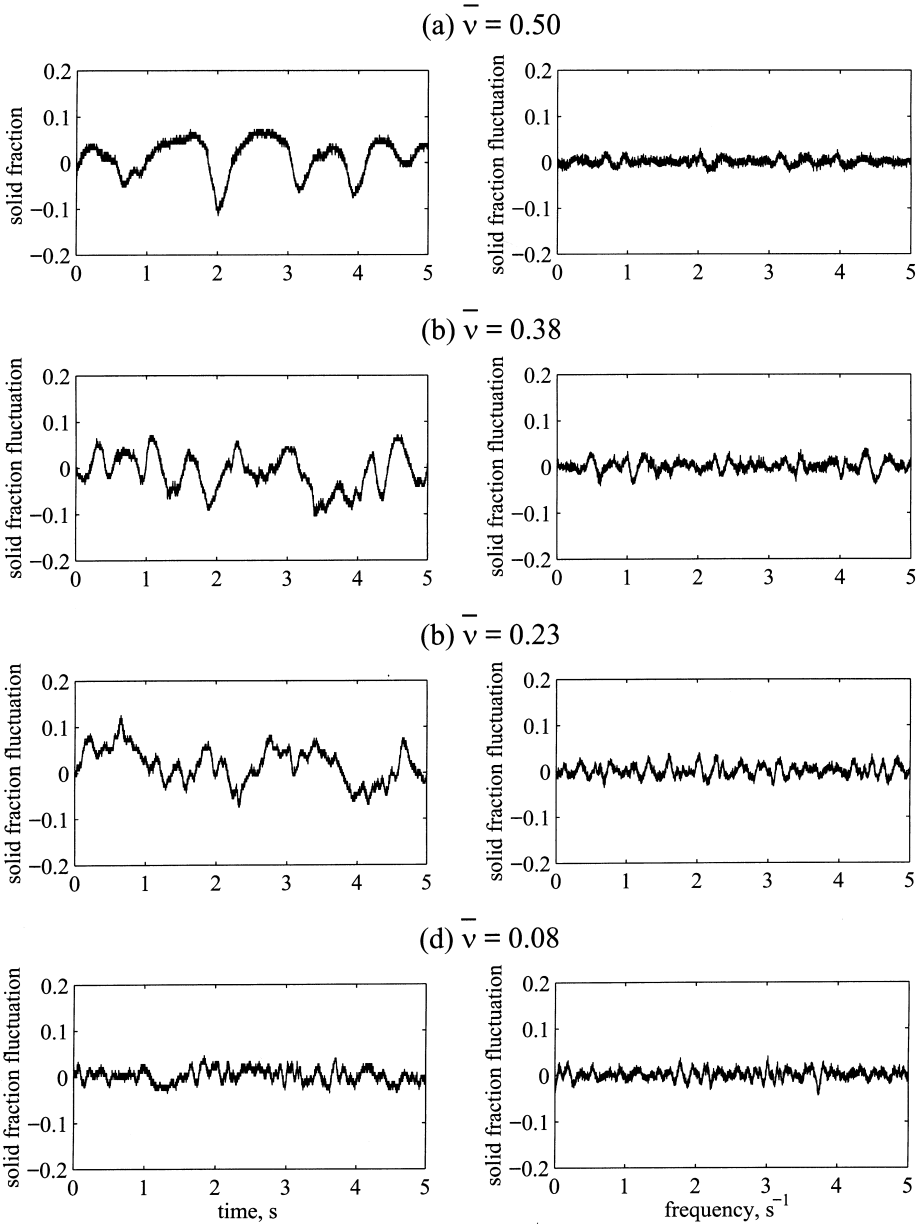

Fig. 11. Effect of the filtering. High pass fourth order Butterworth digital filter, with cut-off frequency of 3 Hz. The original solid fraction fluctuation signal is shown on the left column, the resulting signal after the filtering.

5. Comparisons

Buyevich and Kapbasov (1994) proposed a mathematical model to study the random small-scale fluctuations of particles in a fluid in a macroscopically uniform disperse mixture. The model assumes that momentum is transferred mainly through direct collisions. Assuming that the fluctuations in the system are isotropic and following an analysis inspired by thermodynamic theory of fluctuations, an expression for the mean square number density fluctuations is obtained. The mean square number density fluctuations are found to be related to the granular temperature and the granular chemical potential. From geometric considerations, an expression for the solid fraction fluctuation as a function of the mean solid fraction is derived. Based on a Carnahan–Starling model, it is obtained

$$\overline{\nu'}^2 = \nu^2\left[1 + 2\nu\frac{4-\nu}{(1-\nu)^4}\right]^{-1} \tag{3}$$

where ν is the mean value of the solid fraction, and $\overline{\nu}'^2$ is the mean square solid fraction fluctuation. The authors then discuss the validity of the Carnahan–Starling model for high concentrations. An alternative expression is derived based on the Enskog model for dense gases, leading to

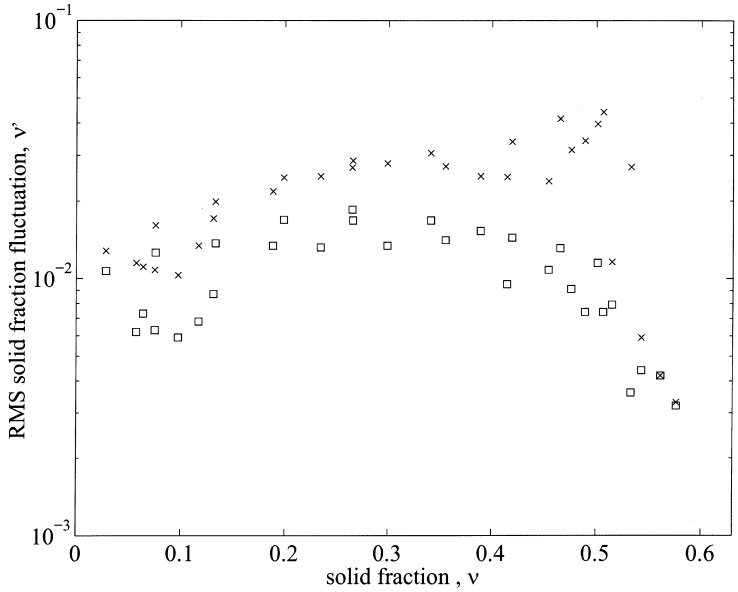

Fig. 12. RMS solid fraction fluctuation as a function of the solid fraction, before filtering (×) and after high-pass filtering (□). Results for 3 mm glass particles in the 5.08 cm and the 10.16 cm test sections.

$$\overline{v'}^2 = v^2\left[1+\left(\frac{v}{v_*}\right)^{1/3}\right]\left[1+\frac{1}{3}\left(\frac{(v/v_*)^{1/3}}{1-(v/v_*)^{1/3}}\right)\right]^{-1} \tag{4}$$

where v_* is the empirical value of solid fraction at close packing.

Eqs. (3) and (4) consider only the small scale fluctuations. Since the large scale fluctuations in the measurements can be filtered out, a direct comparison of the measurements and the predictions is possible. In Fig. 13, a direct comparison of the two curves (Eqs. (3) and (4)) and the experimental measurements is shown. The models appear to predict the shape of the experimental measurements, but the absolute value is over-predicted by a factor of 4 or 5 and almost by an order of magnitude for the case of light particles. Note also that, the predictions do not depend on the particle properties.

The deviation of the measurements and the theoretical predictions increase as the particle inertia decreases. The construction of the model assumes that momentum is transferred through direct collisions but does not account for the effects of the interstitial fluid or particle properties in the particle collisions. Zenit and Hunt (1999) found that the strength of an immersed collision decreases with decreasing particle inertia (particle Stokes number). Clearly,

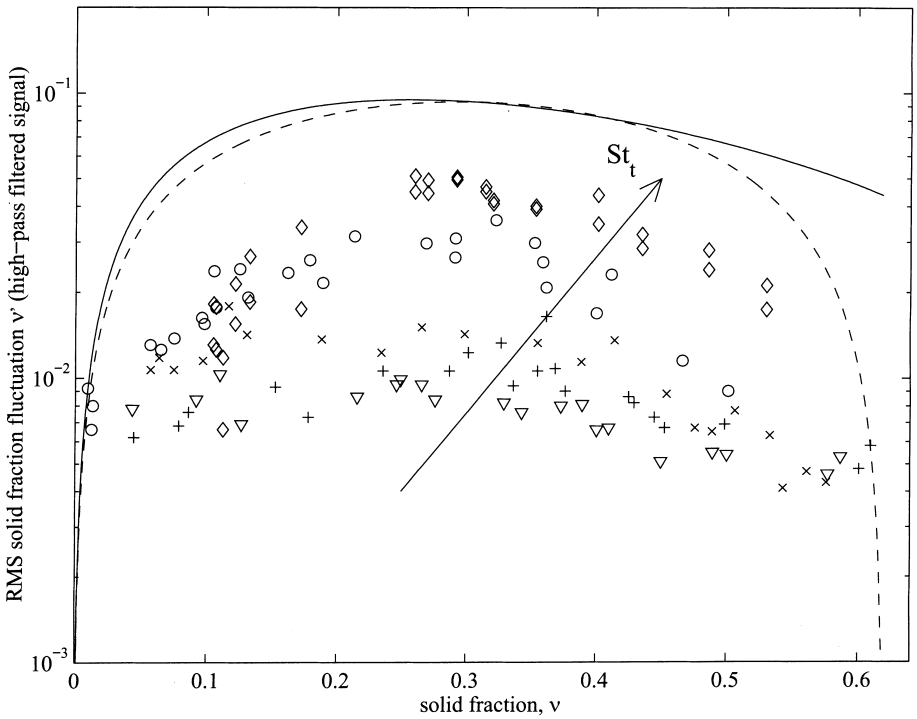

Fig. 13. RMS solid fraction fluctuation after high pass filtering as a function of the solid fraction. All from a 5.08 cm test section fluidized bed. Liquid fluidized particles in a 5.08 cm test section: 3 mm glass particles($\times$, $St_t \approx 70$), 6 mm glass particles ($\bigcirc$, $St_t \approx 730$), 4.5 mm steel particles ($\diamond$, $St_t \approx 2300$), 6.35 mm nylon particles ($\triangledown$, $St_t \approx 100$), and 3.41 mm PVC cylinders ($+$, $St_t \approx 70$). The lines are the predictions from Eq. (3) (solid line), Eq. (4) (dashed line), which can be interpreted to represent the case $St \to \infty$.

this observation supports the idea that direct collisions are the responsible mechanism for the generation of high frequency solid fraction fluctuations and that as the particle inertia increases, the fluctuations are closer to those predicted by dry-collision-based model (which can be interpreted as the case when the particle inertia is infinitely large). Other reasons for the disagreement between the model and the experimental results may arise from the fact that the model assumes an isotropic state of solid fraction fluctuations. In the fluidized bed experiments the fluctuations are not isotropic because the fluid medium flows in the axial direction and has a zero net radial and tangential motion; therefore, the velocities and fluctuations are expected to be larger in the axial direction (Carlos and Richardson, 1968). Also, the model predicts values of the point-wise RMS fluctuation, but the measurements obtained were cross-sectional averages of the solid fraction.

6. Summary and discussion

By analyzing the non-steady component of the volume fraction signal obtained from the impedance volume fraction meter (IVFM), a measure of the agitation in a liquid–solid flow was obtained indicating both high-amplitude low-frequency and low-amplitude high-frequency fluctuations. The low frequency fluctuations appeared as moving wave-like bands of low concentration. The high frequency fluctuations were more random in nature.

When the RMS solid fraction fluctuation for the fluidized beds was plotted as a function of the mean solid fraction, several regimes were observed, which corroborates (by using an different experimental technique) the previously reported results of Didwania and Homsy (1981). Between the closed packed state and 40% solid fraction, the low frequency fluctuations dominated. A maximum was observed at approximately 50% of solids concentration. The low-frequency traveling bands of low density were the main contribution for the appearance of a maximum RMS fluctuation observed at that concentration. This regime was referred to as wavy flow by Didwania and Homsy. For concentrations below 40%, the low frequency fluctuations began to lose coherence and a higher frequency component began to appear, which could be associated with the regime named wavy flow with transverse structure. The RMS fluctuation decreased from its maximum value at 50% solid fraction, reached a local minimum at around 40%. For decreasing concentration, the RMS fluctuation began to increase again and reached a second local maximum at approximately 30% of concentration. The increase on RMS fluctuation was attributed to the increase of high frequency fluctuations. This increase indicates a turbulent-like behavior in accordance with Didwania and Homsy's fine-scale turbulence regime. For concentrations lower than 30% the RMS fluctuation decreased steadily until zero concentration, which can be associated with the last regime, the bubbling state. The values of concentration at which the flow transitions occur in the present experiments are close, but not exactly the same, to those reported by Didwania and Homsy. The difference can be attributed to the differences in experimental setups (2D versus 3D) and particles used.

The results obtained for different particle sizes and densities were compared. The RMS fluctuation appeared to be higher for larger particles. For the same concentration, fluidized beds with larger diameter particles had a higher value of the RMS fluctuation. The only

exception were the 4.5 mm steel particles, the densest particles tested, which showed the highest value of RMS fluctuation for all concentrations. The fluidization velocity for heavy particles is large, implying higher Reynolds number for these flows than for the lighter particles. Hence, turbulent motions may be present in the continuum phase entering the fluidized bed leading to a modified behavior. Didwania and Homsy (1981) only reported values of the RMS solid fraction fluctuation for very concentrated beds, which resulted in limited direct comparison with the present experimental results. Also, only the case of their 1.1 mm ballotine spheres had a terminal Stokes number comparable to those of the particles used in this study. For that case, the RMS solid fraction fluctuations had values within the same range as those presented here.

Measurements were performed in a vertical gravity-driven flow for both cocurrent and countercurrent flows. The same type of behavior was encountered in these flows; however, the flows in countercurrent configuration showed higher values of the RMS fluctuation. Since flows of concentrations higher than 40% were not possible to achieve with the present experimental setup, the maximum RMS value observed in highly concentrated fluidized beds was not observed in the vertical flows. The direction of the fluid phase with respect to that of the solid phase may have an influence in the agitation of the flows. In cocurrent flows both phases move in the same direction and at comparable speeds; therefore, the mixture moves in a plug-type translation. Fluctuations in this case are generated solely by the shear with the containing walls, resulting in a lower value of the RMS fluctuation. In a countercurrent case, in addition to the wall shear, the flow direction of the solid and fluid phases are opposite. The combination of these effect results in higher values of the RMS fluctuation.

To investigate the contribution of each of the two types of fluctuations (low and high frequency) to the total RMS fluctuation, a digital high-pass filter was applied to the time-dependent solid fraction signals. The recalculated value of the RMS fluctuation was smaller than that of the original traces for all solid fractions. The maximum RMS fluctuation observed at 50% of solid fraction disappeared and the other local maximum observed at approximately 30% remained unchanged. Therefore, the first maximum was a result of the low-frequency fluctuations and the second maximum was produced by the high-frequency fluctuations. Additionally, the scaling of the filtered measurements was modified. For a given solid fraction, the fluidized beds with more massive particles (higher terminal Stokes number) appeared to have higher values of the filtered RMS fluctuation, which is interpreted as an indication of the effect of particle collisions as the dominating mechanism for high frequency solid fraction fluctuations.

The trends obtained for the filtered fluctuations resemble the behavior observed in the measurement of collisional particle pressure in liquid fluidized beds (Zenit et al., 1997). In that investigation the collisions of particles in the fluidized media were quantified and averaged to obtain the collision-generated pressure exerted on the containing walls. Low frequency pressure fluctuations were eliminated such that only collisional pressure impulses were taken into account. Like in the case of high-frequency solid fraction fluctuations, the particle pressure was shown to have a maximum value for an intermediate concentration (30% solid fraction). It was also found that the magnitude of the normalized particle pressure appeared to scale with the particle density and the particle's terminal velocity squared. The resemblance between the measurements of particle pressure and high-frequency solid fraction fluctuations supports the

idea that particle collisions are one of the generating mechanisms for high frequency fluctuations in a liquid-solid flows where particles have large inertia.

Acknowledgements

The National Council for Science and Technology of Mexico (CONACYT) is acknowledged for partially supporting R. Zenit during his graduate sojourn at the California Institute of Technology. The help of Elliott Rushing is also acknowledged during the performance of the last set of experiments.

References

Batchelor, G.K., 1988. A new theory of the instability of a uniform fluidized bed. J. Fluid Mech 193, 75–110.

Bernier, R.N., 1982. Unsteady two-phase flow instrumentation and measurement. Ph.D. thesis, California Institute of Technology, Pasadena, CA.

Buyevich, Y.A., Kapbasov, S.K., 1994. Random fluctuations in a fluidized bed. Chem. Engng. Sci 49, 1229–1243.

Carlos, C.R., Richardson, J.F., 1968. Solids movement in liquid fluidized beds. Part I: particle velocity distribution. Chem. Engng. Sci 23, 813–824.

Couderc, J.P. 1985. Incipient fluidization and particulate systems. In: Davidson, J., Clift, R., Harrison, D. (Eds.), Fluidization, 2nd ed. Academic Press, London, pp. 1–46.

Didwania, A.K., Homsy, G.M., 1981. Flow regimes and flow transitions in liquid fluidized beds. Int. J. Multiphase Flow 7, 563–580.

Di Felice, R., 1995. Hydrodynamics of liquid fluidization. Chem. Engng. Sci 50, 1213–1245.

Ham, J.M., Thomas, S., Guazelli, E., Homsy, G.M., Anselmet, M.-C., 1990. An experimental study of the stability of liquid fluidized beds. Int. J. Multiphase Flow 16, 1990.

Jin, C., 1996. Generic stability model and experimental study of liquid-fluidized beds. Ph.D. thesis, University of Southern California, Los Angeles, CA.

Kytömaa, H.K., 1987. Study of the structure in multicomponent flows. Ph.D. thesis, California Institute of Technology, Pasadena, CA.

Kytömaa, H.K., Brennen, C.E., 1986. Some observations of flow patterns and statistical properties of three component flows. J. Fluids Eng 110, 76–84.

Zenit, R., Hunt, M.L., Brennen, C.E., 1997. Collisional particle pressure measurements in solid–liquid flows. J. Fluid Mech 353, 261–283.

Zenit, R., 1998. Collisional mechanics in liquid-solid flows. Ph.D. thesis, California Institute of Technology, Pasadena, CA.

Zenit, R., Hunt, M.L., 1999. Mechanics of immersed collision of particles. J. Fluids Eng 121, 179–184.